NANO · MICRO small
www.small-journal.com

Diffusion Behaviors of Integrins in Single Cells Altered by Epithelial to Mesenchymal Transition

Jing-Wen Yuan, Yu-Ning Zhang, Yu-Ru Liu, Wei Li, Shuo-Xing Dou, Yan Wei, Peng-Ye Wang,* and Hui Li**

Cell morphology and migration depend critically on the adhesions on the extracellular matrix (ECM), determined by the transmembrane protein integrins. The epithelial to mesenchymal transition (EMT) is a prominent transformation process in which adherent cells acquire a mesenchymal phenotype and a promoted migration. EMT plays important roles in embryonic development and cancer metastasis, and its hallmarks include the acquisition of front-back cell polarity and loss of cell–cell contact. However, how integrins dynamically regulate cell-ECM adhesions and cellular behaviors during EMT is still unclear. Using single-particle tracking of β1-integrins labeled with quantum dots, the temporal-spatial on-membrane dynamics of integrins in the EMT of MCF10A cells is revealed. β1-integrins exhibit significantly enhanced dynamics, which temporally behave more diffusive and less immobilized, and spatially become distributed asymmetrically with front regions being more dynamic. These dynamic alterations are shown to arise from microtubule remodeling in EMT. The results shed new light on the EMT mechanism from the cell-ECM adhesion perspective, and suggest that the enhanced integrin diffusion may represent as a new hallmark of EMT.

1. Introduction

Cell properties and behaviors are widely regulated by extracellular matrix (ECM).[1] Transmembrane protein integrins, as a key component of cell adhesions connecting cells to ECM, are crucial for cell morphology and migration through their dynamic translocations on cell membranes, and subsequent participations in the assembly and disassembly of focal adhesions at specific times and locations.[2] Epithelial to mesenchymal transition (EMT) is a biological process in which epithelial cells acquire a mesenchymal phenotype and a promoted migration, which is important in embryonic development, wound healing and cancer metastasis.[3] In cancer, EMT is recognized as the first step of tumor invasion and metastasis, and associated with the therapy resistance. The hallmarks of EMT include the acquisition of front-back cell polarity by remodeling cytoskeletons and the loss of cell-cell contacts by decreasing E-cadherin expression.[3a,b] Despite the current knowledge in cellular phenotype and cell-cell contact for EMT, however, the cell-ECM adhesions in EMT, especially the dynamic behaviors of integrins in mediating the adhesions, remain to be elucidated. To unravel integrin dynamics during EMT, a combination of the single-particle tracking (SPT) method with reliable integrin-labeling strategies and an effective analytic method for temporal-spatial dynamics is necessary.[4] Here, using these methods together with quantum dot (QD)-labeled integrins, we examined the diffusion dynamics of integrins on cell membranes during EMT in MCF10A cells. We discovered that integrins exhibit significantly enhanced dynamics after EMT, which temporally behave more

J.-W. Yuan, Y.-R. Liu, W. Li, S.-X. Dou, P.-Y. Wang
Beijing National Laboratory for Condensed Matter Physics and Laboratory of Soft Matter Physics
Institute of Physics
Chinese Academy of Sciences
Beijing 100190, China
E-mail: pywang@iphy.ac.cn

J.-W. Yuan, S.-X. Dou, P.-Y. Wang
School of Physical Sciences
University of Chinese Academy of Sciences
Beijing 100049, China

Y.-N. Zhang
Department of Orthodontics
Peking University School and Hospital of Stomatology
Beijing 100081, China

The ORCID identification number(s) for the author(s) of this article can be found under https://doi.org/10.1002/smll.202106498.

DOI: 10.1002/smll.202106498

W. Li, P.-Y. Wang
Songshan Lake Materials Laboratory
Dongguan, Guangdong 523808, China

Y. Wei
Beijing Laboratory of Biomedical Materials
Department of Geriatric Dentistry
Peking University School and Hospital of Stomatology
Beijing 100081, China
E-mail: kqweiyan@bjmu.edu.cn

H. Li
School of Systems Science and Institute of Nonequilibrium Systems
Beijing Normal University
Beijing 100875, China
E-mail: huili@bnu.edu.cn

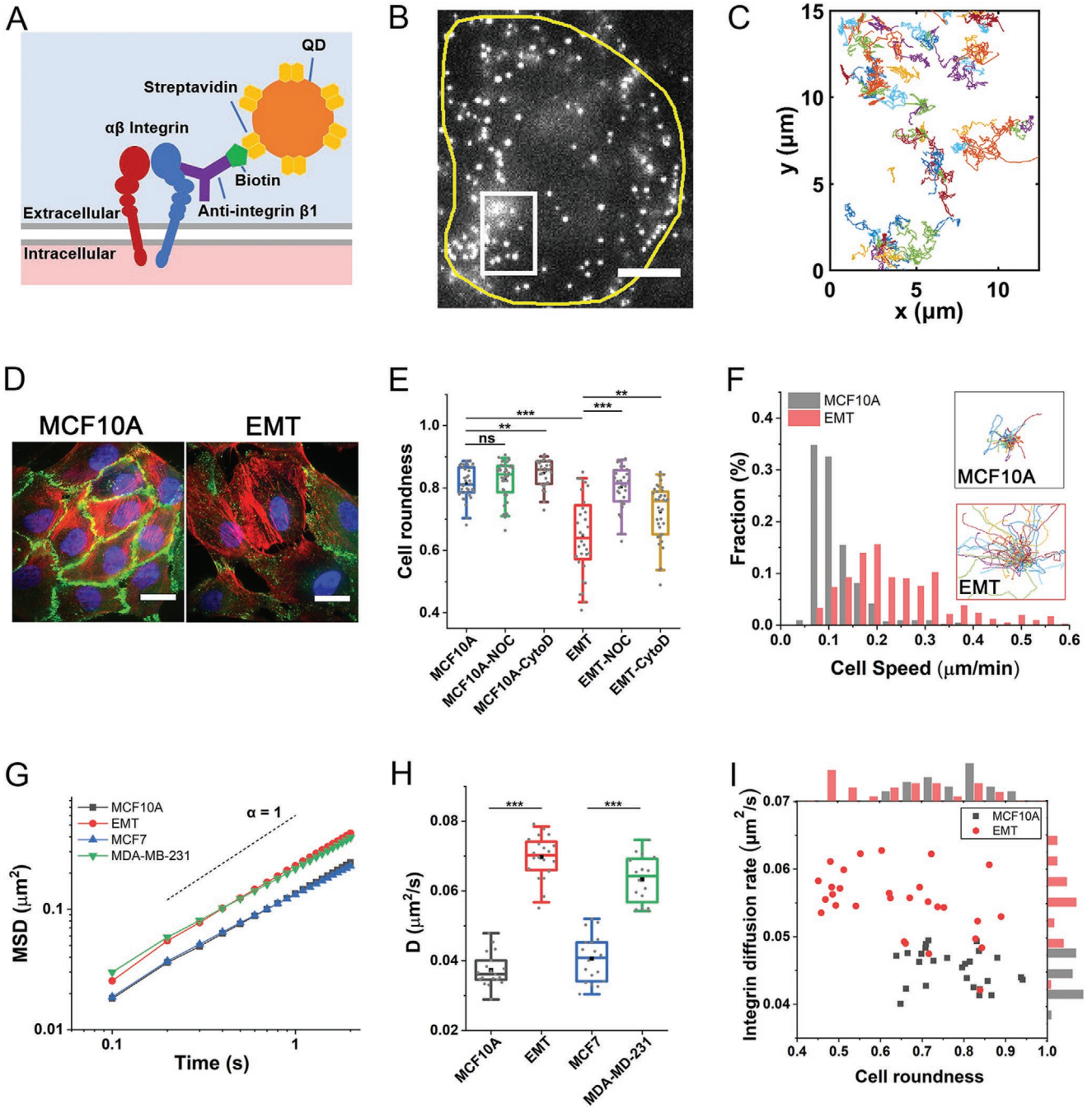

Figure 1. β1-integrins exhibit significantly enhanced diffusion dynamics in the EMT of MCF10A cells. A) Labelling of β1-integrins by biotinylated β1-integrin antibody and streptavidin–quantum dots consecutively on cell membranes. B) Fluorescence images of QD-labeled β1-integrins in an MCF10A cell. The cell boundary is marked by the yellow line. Scale bar, 10 μm. C) β1-integrin trajectories within the box area indicated in (B). D) Merged images of nuclei (blue), actin (red) and E-cadherin (green) in MCF10A cells before and after EMT. Scale bar, 20 μm. E) Comparisons of cell roundness in MCF10A, EMT, and cells treated with nocodazole (NOC) or cytochalasin D (CytoD). F) Comparison of cell speed between MCF10A (n = 435) and EMT (n = 441) cells. Insert, representative trajectories recorded over 40 min. G,H) Averaged MSD and diffusion rates from the trajectories of QD-labeled β1-integrins in MCF10A (3312 trajectories, 20 cells), EMT-treated (10 697, 20), MCF7 (2123, 18) and MDA-MB-231 cells (18 323, 16). I) The diffusion rate of integrins enables better identification of EMT cells than the morphological roundness of cells. MCF10A (n = 27), EMT (n = 29) cells. The boxes represent the interquartile range between 75% and 25%, where the whiskers represent the 95% and 5% values, and the black squares represent the average. $^{**}P < 0.01$, $^{***}P < 0.001$; ns, not significant. Error bars indicate the SEM.

diffusive and less immobilized, and spatially become distributed asymmetrically. We further demonstrated that these alterations in integrin dynamics primarily resulted from microtubule remodeling during EMT. Our results suggest an important role of β1-integrin dynamics in EMT-promotes cell migration and provide new insight into how molecular dynamics is coupled

to cellular behaviors. The enhancement in integrin diffusion dynamics may represent as a new hallmark of EMT.

2. Results and Discussion

To track the integrin movements, individual β1-integrin proteins on membranes of nontumorigenic MCF10A cells were labeled using biotinylated β1-integrin antibodies and streptavidin–QDs consecutively at 4 °C, and then the cells were allowed to recover at 37 °C before imaging (**Figure 1**A). This labeling method enables individual integrins to link the QDs with outstanding photostability at a 1:1 ratio, which is essential for the long-term single-molecule imaging of integrins in living cells (Figure 1B). The amount of QD-labeled β1-integrins was determined to be 157 ± 12 in single MCF10A cells (Figure S1, Supporting Information). Moreover, the QD-labeled β1-integrins were observed to participate in the formation of adhesion at the protrusive leading edge (Figure S2, Supporting Information), demonstrating that the labeling method does not influence the function of integrins or cell migration.[5] Then, we performed continuous imaging of single QD-labeled β1-integrins at a speed of 10 Hz, with their trajectories extracted from the video (Figure 1C).

The EMT in MCF10A cells was induced by adding 5 ng mL^{-1} transforming growth factor β (TGF-β), a commonly used method.[3b,6] Hallmarks of EMT were observed 72 h after induction: E-cadherin, a biomarker of intercellular connections, disappeared at the cell boundaries (Figure 1D), and cell morphology gradually changed from polygonal to spindle-liked (Figure 1E and Figure S3, Supporting Information). Furthermore, we found that EMT significantly promoted cell motility (Figure 1F and Figure S4, Supporting Information). Taken together, the changes in cell morphology, loss of E-cadherin and promotion of cell motility indicate that EMT was successfully induced in MCF10A cells.

Using SPT of β1-integrins, surprisingly, the mean square displacement (MSD) analysis shows that integrins diffuse faster in EMT-induced MCF10A cells than in untreated ones (Figure 1G), with diffusion rates increasing from 0.039 to 0.070 $\mu m^2\ s^{-1}$ (Figure 1H). The measured diffusion rates are consistent with the results reported in other cell lines.[7] To further examine the enhanced dynamics of integrins in EMT, we compared integrin dynamics between MCF7 and MDA-MB-231 cells, which represent standard epithelial and mesenchymal cells respectively (Figure 1G–H). We found that β1-integrins diffused faster on MDA-MB-231 cells than on MCF7 cells, with diffusion rates of 0.063 and 0.041 $\mu m^2\ s^{-1}$, respectively. Interestingly, the difference in integrin dynamics is in good agreement with the difference between MCF10A and EMT cells. These results demonstrate that the enhancement of β1-integrin diffusion is a general feature in EMT.

Activation of integrins is known to appear as immobilization on the cell membrane and is connected to the ECM and intracellular components, such as talins.[2c,8] Indeed, using dual-color imaging of both QD-labeled integrins and GFP-labeled talins, we observed that integrin diffused to sites with talin and was then immobilized there (**Figure 2**A). To resolve the temporal dynamics of integrins containing altered diffusive and immobilized motions, we applied an automatic method to identify the two motion modes from the whole trajectories.[9] As shown in Figure 2B, a local MSD was calculated to determine the temporal diffusion rates and exponent α along the trajectory. The exponent α indicates the nonlinear relationship of MSD over time, in which an α of ≈1 indicates Brownian motion and an $\alpha < 1$ indicates subdiffusion and confined motion.[10] The segments of immobilized motion are identified when the temporal diffusion rate is less than 0.015 $\mu m^2\ s^{-1}$, and the classification results are illustrated in Figure 2A. To further verify our method, we applied Mn^{2+} to activate β1-integrin by stabilizing their active conformation, which causes the immobilization of integrins.[11] We observed increased immobilized β1-integrins (Figure 2C), demonstrating that the classification method is effective and that immobilized motion of β1-integrin is associated with integrin activation.

Using the temporally analytical method, we unexpectedly found that the fraction of immobilized motion of β1-integrins decreases after EMT, and the integrins are inclined to diffuse on the membrane (Figure 2D). Moreover, the classified mobile segments of β1-integrins exhibit an increased diffusion rate after EMT, whereas the immobile parts are similar (Figure 2E). In addition, we found that the decreased immobilization of β1-integrins observed in EMT experiments agrees with the comparison between MCF7 and MDA-MB-231 cells, in which the β1-integrins in mesenchymal MDA-MB-231 cells exhibit a reduced fraction of immobilized motion (Figure 2D). Taken together, our results suggest that β1-integrins move diffusively and are less immobilized in EMT cells. As such, there is one interesting question: how do EMT cells migrate faster than MCF10A cells if integrins were less immobilized and then activated? To this end, we quantified the total number of immobilized events of β1-integrins per cell and found that it increased by 40% after EMT induction (Figure S5, Supporting Information). This suggests that the total events of β1-integrins that may participate in adhesion formation actually increase in EMT cells, which could contribute to EMT-induced cell movements. It is likely resulted from the upregulated expression of integrins in response to TGF-β treatment,[12] as evidenced by the more QD-labeled β1-integrins observed in EMT cells (Figure S1, Supporting Information).

Next, we investigated the spatial characteristics of integrin dynamics by plotting the diffusion map and exponent α map of β1-integrins in single cells.[13] Briefly, the spatial diffusion rate D_p and exponent α_p at each point within the cell coverage are calculated using the segments of trajectories around the point. We observed heterogeneous diffusive dynamics of integrins in both MCF10A and EMT cells (**Figure 3**A,B). Notably, compared to the symmetrical map in MCF10A cells, EMT cells display polarities in both D_p and α_p maps for β1-integrins. A quantitative analysis further demonstrated that the values of D_p and α_p at the front region are markedly larger than those at the rear region in EMT cells compared to MCF10A cells (Figure 3C–D). This indicates that β1-integrins are more diffusive at the front region ($\alpha_p \approx 1$), while they are subdiffusive and immobile at the rear region ($\alpha_p \approx 0.5$). Therefore, our results suggest that symmetrical breaking emerges in the spatial dynamics of integrins during EMT.

Cytoskeletal remodeling, a hallmark of EMT, is tightly correlated with cell migration and integrin involvement.[3b,14] To

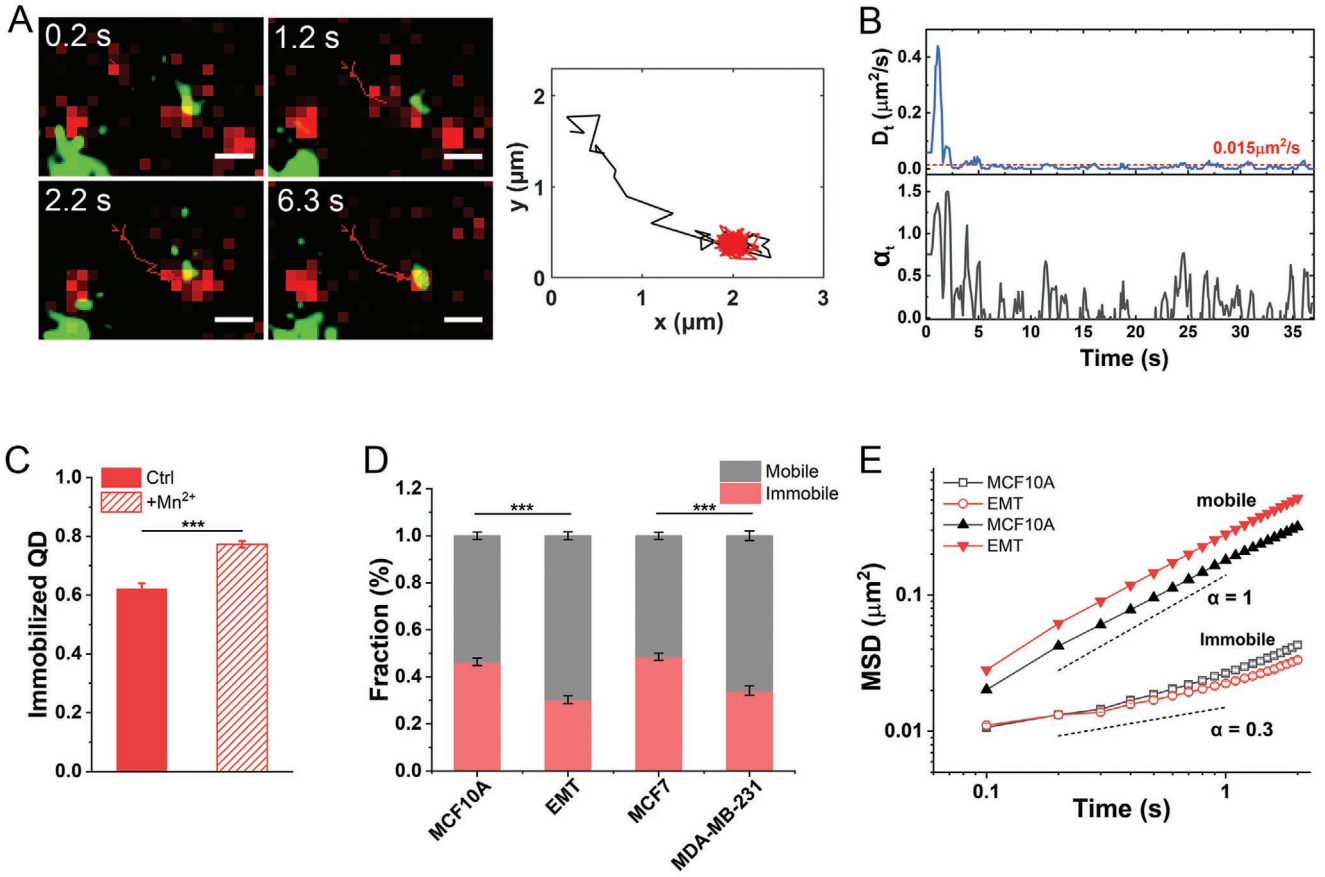

Figure 2. Temporal dynamics of β1-integrins reveals the reduced fraction of immobilization after EMT. A) Image serials of a QD-labeled β1-integrin (red) overlaid with GFP-labeled talin (green) (left panel). The integrin trajectory consists of mobile (black) and immobile (red) motions (right panel). Scale bar, 1 μm. B) The temporal diffusion rate D_t and exponent α_t at each point of the trajectory shown in (A). Points with D_t below 0.015 $\mu m^2 s^{-1}$ are regarded as immobile segments. C) Mn^{2+} addition increased the immobilized QDs in MCF10A cells. The cells were treated with 0.1×10^{-3} M Mn^{2+} for 20 min. MCF-10A (5951 trajectories, 12 cells) and Mn^{2+} treated (2546, 12) cells. D) Fraction of mobile and immobile segments of β1-integrins in MCF10A (3312 trajectories, 20 cells), EMT (10 697, 20), MCF7 (2123, 18) and MDA-MB-231 (18 323, 16) cells. E) Averaged MSD of mobile and immobile trajectory segments in cells before and after EMT induction. Dashed lines indicate logarithmic slopes of 1 and 0.3. ***$P < 0.001$. Error bars indicate the SEM.

explore the reason for enhanced integrin dynamics in EMT, we applied specific drugs to interfere with MTs and actin filaments. We observed that the disruption of actin filaments by cytochalasin D (CytoD) slightly enhanced the diffusion rate of β1-integrins in both MCF10A and EMT cells (**Figure 4**A,B), which is consistent with the fact that the actin cortex beneath the cell membrane impedes protein diffusion on the membrane.[15] However, disrupting MTs using nocodazole (NOC) significantly decreased integrin diffusion rates by 30% in EMT cells, while it had no effect in MCF10A cells (Figure 4A,B). The decreased integrin dynamics in NOC-treated EMT cells approaches to that observed in MCF10A cells. In addition to diffusion on cell membranes, integrins may endocytose and undergo vesicular transport.[16] To examine whether the observed integrin dynamics are associated with MT-based intracellular transport, we used specific drugs to inhibit clathrin-dependent and caveolae-dependent endocytosis[17] and found no obvious difference in integrin dynamics (Figure S6, Supporting Information), demonstrating that the integrins mainly underwent diffusion on cell membrane in our experiments. Further analysis of the temporal dynamics of integrins shows that a greater fraction of immobile motion occurred in NOC-treated EMT cells (Figure 4C). Spatially, it is observed that the pre-existing polarity of integrin dynamics remains the same in CytoD-treated EMT cells without actin filaments (Figure 4D and Figure S7, Supporting Information). However, the polarity is eliminated when MT is disrupted (Figure 4D and Figure S7, Supporting Information), which is similar to the loss of morphological polarity observed in NOC-treated EMT cells (Figure 1C).

These results indicate that MTs play key roles in enhancing the integrin dynamics in EMT. Unlike the uniform distribution of MTs in MCF10A cells, more MTs appeared at protrusive regions and constituted MT-based lamellipodia in EMT cells (Figure S8, Supporting Information). MTs were reported to contact focal adhesions and facilitate their turnover dynamics.[12,18] Therefore, under the influence of more MTs in EMT cells, less amount of integrins reside in adhesions but more integrins behave diffusively on cell membranes, which increases overall integrin dynamics. Moreover, the appearance of MTs at the front protrusive region makes the integrins more dynamical compared to the rear cell region, generating the spatial polarity of integrin dynamics. Conversely, MT depolymerization by

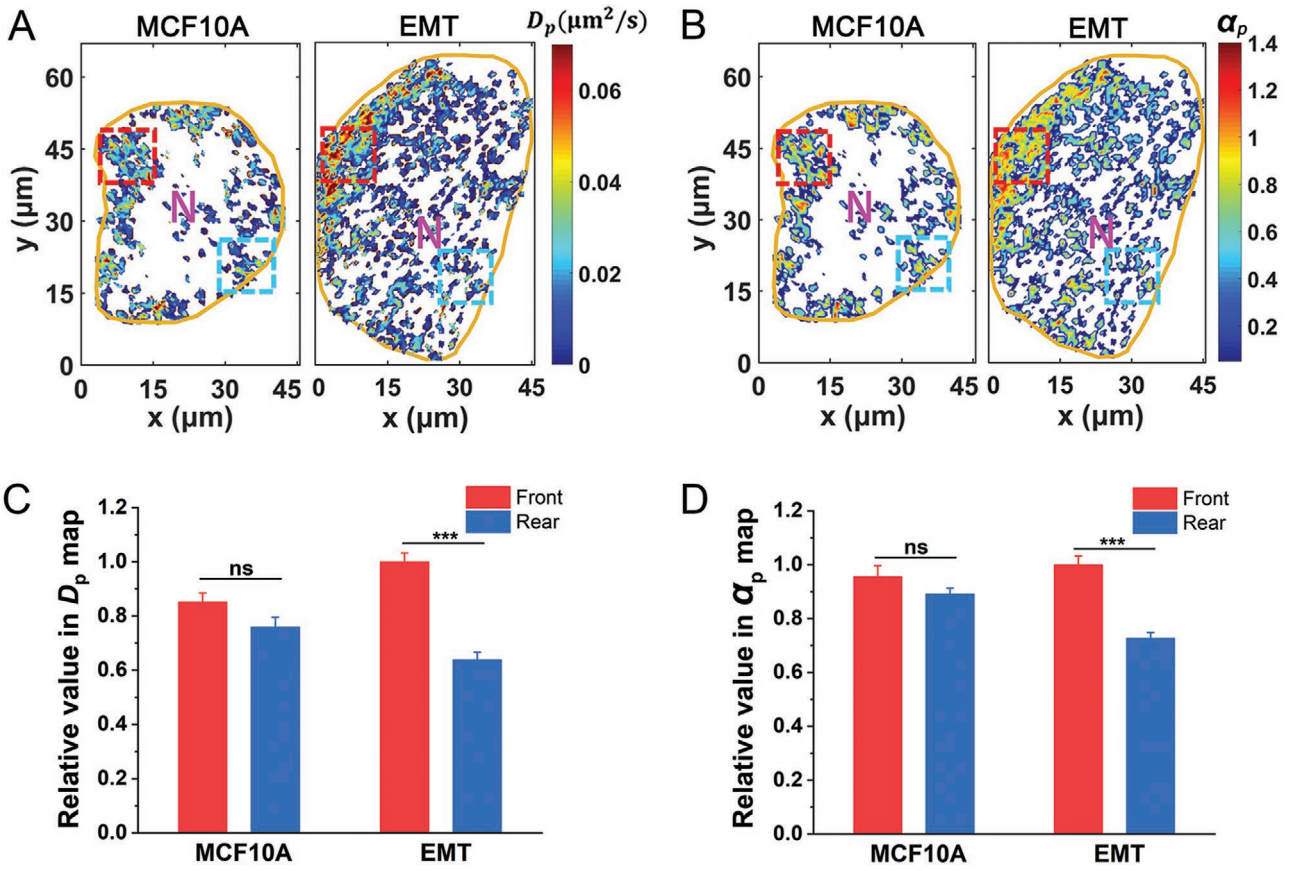

Figure 3. Spatial dynamics of β1-integrins reveals a front-back polarity in EMT cells. Comparisons of A) integrin dynamics by the diffusion rate D_p map and B) the exponent α_p map between MCF10A and EMT cells. C,D) Statistical comparisons show that the front part of EMT cells has increased diffusion rate D_p and exponent α_p compared to the rear part. For each cell, two square areas (12×12 μm^2) at the front and rear regions of a cell are selected respectively, and then the relative values of averaged diffusion parameters within the square areas are compared. MCF10A ($n = 11$), EMT ($n = 11$) cells. ***$P < 0.001$; ns, not significant. Error bars indicate the SEM.

NOC would cause a reduction in lamellipodia and the formation of additional large FAs,[19] resulting in the more immobilized integrins therein (Figure 4C) and the disappearance of spatial polarity in integrin dynamics (Figure 4D and Figure S7, Supporting Information).

3. Conclusions

In this work, using SPT of QD-labeled β1-integrins and temporal–spatial dynamic analysis, we for the first time discovered the enhanced integrin diffusion after EMT, revealing an important role of cell-ECM adhesions in EMT. β1-integrins temporally behave more diffusively and less immobilized and spatially exhibit a polar dynamic distribution in EMT cells. We further demonstrated that MT reorganization leads to the alternations in integrin dynamics. Previously, cytoskeletal remodeling was widely recognized in EMT, especially the change from an actin-rich to a vimentin-rich network.[3c,14] Here, we highlighted the importance of MT in EMT. Moreover, the temporal-spatial integrin dynamics shed new light on the mechanism of EMT-promoted migration. The temporal enhancement in integrin dynamics may facilitate the translocation of integrins to the leading edge, which could facilitate the formation of initial adhesions at the protrusion. The spatial polarity of integrin dynamics could generate bias adhesions in a cell, driving the bias migration.

Furthermore, the identification of EMT cells from the population by current phenotypical and biochemical measurements is still challenging due to cell heterogeneity and plasticity.[20] Compared to phenotypical features which are sensitive to cell culture conditions, the integrin diffusion dynamics is more stable and robust (Figure S9, Supporting Information). Thus, our finding of enhanced integrin diffusion by EMT provides a novel method to identify mesenchymal cells from epithelia cells. This has been verified both by successfully distinguishing between EMT-induced and MCF10A cells (Figure 1I), and between MDA-MB-231 and MCF-7 cells (Figure S10, Supporting Information). We thus expect that the enhanced integrin diffusion may serve as a new hallmark of EMT and offer a diagnose method for malignant tumor cells.[21]

4. Experimental Section

Cell Culture and Drug Treatment: MCF10A cells (ATCC) were cultured in DMEM/F12 (Gibco) with 5% horse serum (Invitrogen), 1% penicillin–streptomycin (Invitrogen), 20 ng mL^{-1} EGF (PeproTech), 0.5 mg mL^{-1} hydrocortisone (Sigma), 100 ng mL^{-1} cholera (Sigma) and 10 ng mL^{-1}

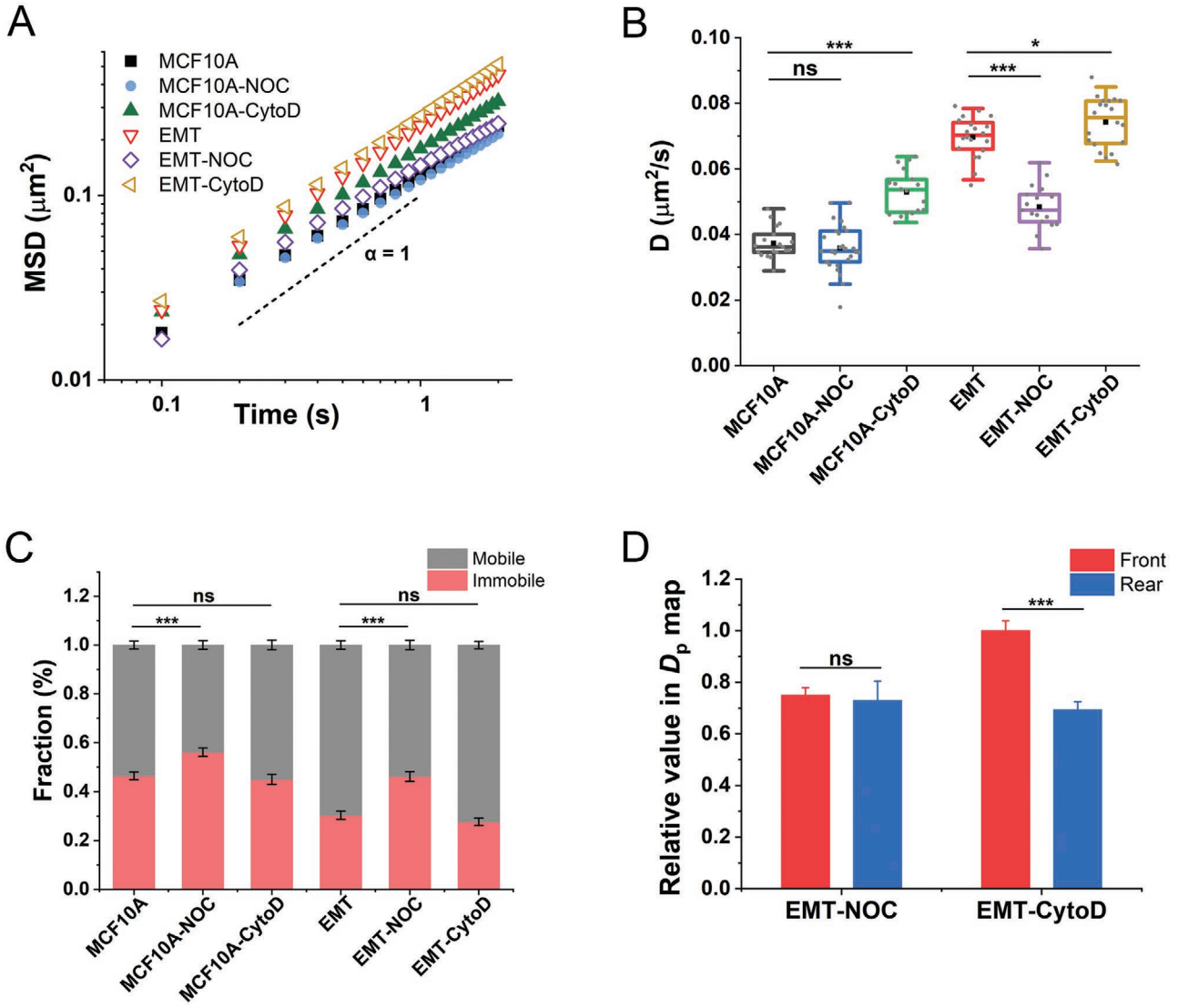

Figure 4. Microtubules play important roles in enhancing integrin dynamics during EMT. A) Averaged MSD, B) diffusion rates, and C) fraction of motion modes of β1-integrin dynamics in MCF10A (3312 trajectories, 20 cells), NOC-treated (1517, 20) and CytoD-treated MCF10A cells (4205, 17) and in EMT (10 697, 20), NOC-treated (2828, 17) and CytoD-treated EMT cells (4240, 20). The boxes represent the interquartile range between 75% and 25%, where the whiskers represent the 95% and 5% values, and the black squares represent the average. D) Statistical analysis of the spatial diffusion rates of integrins shows that the difference between the front and rear parts was eliminated in NOC-treated EMT cells ($n = 10$), while it remains polarized in CytoD-treated EMT cells ($n = 11$). *$P < 0.05$, ***$P < 0.001$; ns, not significant. Error bars indicate the SEM.

insulin (Sigma) at 37 °C and 5% CO_2. Prior to imaging, cells were seeded on the bottom of petri dishes on coverglass. To induce EMT, MCF10A cells were treated with 5 ng mL^{-1} transforming growth factor β1 (TGF-β, Abcam) for 72 h. To disrupt the cytoskeleton, cells were treated with 1×10^{-6} M nocodazole (Sigma) for 20 min to disrupt microtubules or with 1×10^{-6} M cytochalasin D (Sigma) for 20 min to disrupt actin filaments. To activate integrins, cells were treated with 0.1×10^{-3} M $MnCl_2$ solution for 10 min. To inhibit different types of endocytosis of integrins, cells were treated with 100×10^{-6} M monodansylcadaverine (MDC) for 1 h to inhibit clathrin-dependent endocytosis or with 2×10^{-3} M methyl-β-cyclodextrin (MBCD) for 1 h to inhibit caveolae-dependent endocytosis.

Integrin Labeling: β1-integrins on cell membranes were first labeled with 1×10^{-9} M anti-ITGB1 monoclonal antibody conjugated to biotin (MEM-101A, Abcam) on ice in serum- and phenol red-free culture medium for 15 min. The cells were washed with cold PBS solution 3 times and then labeled with 0.5×10^{-9} M streptavidin-QDs (CdSe/ZnS, 655 nm, Invitrogen) for 5 min. After washing the unlabeled QDs 3 times with cold PBS, the cells were incubated in serum-free and phenol red-free culture medium for imaging. Then, the petri dish was transferred to the cell incubator to recover for 15 min before imaging.

Microscope: Fluorescence images using an inverted optical microscope (Olympus IX73) with a 60× oil-immersed objective (1.45 N.A., Olympus) and a back-illuminated EMCCD camera (DU-897 Ultra) were acquired. To maintain cell physiology, an on-stage incubator was installed on the microscope to supply 37 °C and 5% CO_2 during imaging. Three lasers were applied to image the different probes: a 561-nm laser (Sapphire 561, Coherent) for QDs or Alexa 594; a 488-nm laser (Sapphire 488, Coherent) for Alexa 488 or GFP; and a 405 nm laser (OBIS 405, Coherent) for Hoechst 33342. The on–off state of the lasers was controlled by mechanical shutters (Uniblitz LS6T2). To perform dual-color imaging, a dual-channel simultaneous imaging system (DV2, Photometrics) was used to image both the QDs and GFP at the same time. Total internal reflection fluorescence (TIRF) and highly inclined

and laminated optical sheet (HILO) imaging were both performed to track single molecules. The movements of QD-labeled β1-integrins were recorded with a total of 2000 frames at 10 Hz. The pixel size is 0.2667 µm. The localization accuracy is determined to be 37 nm.

Single-Particle Tracking of QDs: The ImageJ plugin Particle Tracker to track single QDs from the videos was used, as previously described. Briefly, the radius, cut-off, and percentile parameter were adjusted to extract individual particles. A cut-off parameter was set to exclude fuzzy or aggregated particles, and a percentage was set to distinguish particles from the background. Second, the linking range and displacement parameters were adjusted to connect the particle positions between frames. To solve the problem of QD blinking, the parameter of linking range is set to 2, to bridge over the QD blinking events. All detection and linking were visually checked. Trajectories longer than 30 frames were saved in text files for further analysis.

Temporal Analysis of Integrin Dynamics: A custom-written algorithm in MATLAB to analyze the integrin trajectories was used. The mean square displacement (MSD) of each trajectory was calculated using the equation $\mathrm{MSD}(\tau) = \langle |r(t+\tau) - r(t)|^2 \rangle$, where τ is the time lag. From the MSD, the diffusion rate D is determined by linear fitting of the first three points by $\mathrm{MSD}(\tau) = 4D\cdot\tau + c$. The exponent α is determined using the nonlinear fitting of all the points by $\mathrm{MSD}(\tau) = A\cdot\tau^{\alpha}$, which also corresponds to the slope of the MSD curve in the log–log plot. The value of the exponent α is between 0 and 2, in which an α of ≈1 indicates Brownian motion and an $\alpha < 1$ indicates subdiffusion and confined motion. To analyze the temporal dynamics of integrins and distinguish the immobile segments within an integrin trajectory, the temporally local MSD with a window size of 20 points along the trajectory was calculated. The temporal diffusion D_t and exponent α_t for each point in the trajectory were determined by fitting the local MSD with the similar equations mentioned above. To distinguish immobile motion, movements with a D_t less than 0.015 µm ^{2} s^{-1} were regarded as immobilization, corresponding to the region explored by an integrin in 1 s being smaller than one pixel area (0.2667 µm) ^{2}. When consecutive points with D_t less than 0.015 µm ^{2} s^{-1} were longer than 5 points, these points were classified as a segment of immobile motion.

Spatial Analysis of Integrin Dynamics: To analyze the spatial dynamics of integrins, the plotting of spatial maps of integrin dynamics on a cell was achieved using a custom-written algorithm in MATLAB, as previously described. Briefly, the area of the cell was divided into a square grid. Each grid point was the unit of the spatial map, and the grid size corresponded to the spatial resolution of the map. In the experiment, the grid size was chosen to be 2 pixels, and the distance threshold was set to 1.5 pixels by considering the diffusion rate of integrins. To calculate the spatial dynamics at each grid point, spatially local trajectory segments were first selected within a distance threshold to the grid point. Then, the spatially local MSD for each grid point was calculated using these segments separately. Next, the spatial diffusion coefficient D_p and exponent α_p at each grid point were determined by fitting the spatially local MSD curves with the equations mentioned above. Finally, the contour maps of the diffusion coefficient D_p and exponent α_p were plotted in MATLAB using a built-in smoothing process. The blank regions or white points in these maps indicated that there was no sufficient integrin trajectory for calculating the locally diffusion dynamics.

Tracking and Analysis of Cell Migrations: The cells were sparsely seeded into a petri dish one day before the experiments. Before imaging, the cell nucleus was stained using Hoechst 33342. Then, the cells were imaged using epifluorescence illumination and a 10× objective every 20 s for 2 h. After that, the trajectory for each cell was extracted using the ImageJ plugin Particle Tracker, in which all detection parameters were adjusted to fit the cell nucleus, and the linking parameters were optimized to fit the cell speed. To analyze the dynamics of cell migration, MSD and diffusion rates for single cells were calculated using the same equations as those for analyzing the integrins.

Immunostaining: Cells were first fixed at room temperature in 4% paraformaldehyde (PFA) for 1 h. After washing with PBS 3 times, the cells were permeabilized with 0.2% Triton X-100 in PBS. Then, the cells were washed with PBS 3 times and blocked in 1% BSA for 1 h at room temperature. For the two-step labeling of E-cadherin and microtubules, primary antibodies, such as anti-E-cadherin nonclonal antibody (1:400, Invitrogen) or rat antitubulin monoclonal antibody (1:500, Abcam), were added to the cells and incubated overnight at 4 °C. Then, after washing with PBS 3 times, the cells were incubated with secondary antibodies, e.g., Alexa-488 goat anti-rat IgG (1:300, Invitrogen) or anti-mouse IgG (1:400, Invitrogen), for 1 h at room temperature. Before imaging, the cells were washed 3 times. The actin filaments were directly labeled with Alexa 594 phalloidin (1:400, Invitrogen) for 1 h. The chromosomes were stained with Hoechst 33342 (1:10 000, Invitrogen) for 10 min at 37 °C.

Image Processing: All image processing was performed using ImageJ software. The boundaries of cells were manually selected in DIC images, and the morphological parameters were measured using ImageJ. Cell roundness was calculated using 4π*area/perimeter^2, with a value of 1 indicating a perfect circle.

Statistics: Comparisons were performed using a two-sample *t*-test: *$P < 0.05$; **$P < 0.01$; ***$P < 0.001$; ns, not significant. All the measurements were taken in three independent experiments.

Supporting Information

Supporting Information is available from the Wiley Online Library or from the author.

Acknowledgements

This work was supported by the National Natural Science Foundation of China (12122402, 12074043, 11874415), the National Key Research and Development Program (2016YFA0301500), Youth Innovation Promotion Association of CAS (2019006).

Conflict of Interest

The authors declare no conflict of interest.

Data Availability Statement

The data that support the findings of this study are available from the corresponding author upon reasonable request.

Keywords

dynamics, epithelial-mesenchymal transformation (EMT), integrins, quantum dots, single-particle tracking

Received: October 26, 2021
Revised: November 25, 2021
Published online: December 18, 2021

[1] a) N. M. Alves, I. Pashkuleva, R. L. Reis, J. F. Mano, *Small* **2010**, *6*, 2208; b) G. Brusatin, T. Panciera, A. Gandin, A. Citron, S. Piccolo, *Nat. Mater.* **2018**, *17*, 1063; c) K. P. McCreery, X. Xu, A. K. Scott, A. K. Fajrial, S. Calve, X. Ding, C. P. Neu, *Small* **2021**, *17*, 2006699; d) S. Jiang, H. Li, Q. Zeng, Z. Xiao, X. Zhang, M. Xu, Y. He, Y. Wei, X. Deng, *Adv. Sci.* **2021**, *8*, 2004000; e) H. Li, Y. Zheng, Y. L. Han, S. Cai, M. Guo, *Proc. Natl. Acad. Sci. USA* **2021**, *118*, e2100697118.

[2] a) R. Changede, H. Cai, S. J. Wind, M. P. Sheetz, *Nat. Mater.* **2019**, *18*, 1366; b) O. Lieleg, M. Lopez-Garcia, C. Semmrich,

J. Auernheimer, H. Kessler, A. R. Bausch, *Small* **2007**, *3*, 1560; c) T. Orre, O. Rossier, G. Giannone, *Exp. Cell Res.* **2019**, *379*, 235; d) S. SenGupta, C. A. Parent, J. E. Bear, *Nat. Rev. Mol. Cell Biol.* **2021**, *22*, 529.

[3] a) R. Kalluri, R. A. Weinberg, *J. Clin. Invest.* **2009**, *119*, 1420; b) J. P. Thiery, H. Acloque, R. Y. Huang, M. A. Nieto, *Cell* **2009**, *139*, 871; c) I. Y. Wong, S. Javaid, E. A. Wong, S. Perk, D. A. Haber, M. Toner, D. Irimia, *Nat. Mater.* **2014**, *13*, 1063.

[4] Z. Wang, X. Wang, Y. Zhang, W. Xu, X. Han, *Small* **2021**, *17*, 2005133.

[5] a) N. Arora, A. Syed, S. Sander, E. A. Smith, *Phys. Biol.* **2014**, *11*, 066001; b) O. Rossier, V. Octeau, J. B. Sibarita, C. Leduc, B. Tessier, D. Nair, V. Gatterdam, O. Destaing, C. Albiges-Rizo, R. Tampe, L. Cognet, D. Choquet, B. Lounis, G. Giannone, *Nat. Cell Biol.* **2012**, *14*, 1057.

[6] J. Xu, S. Lamouille, R. Derynck, *Cell Res.* **2009**, *19*, 156.

[7] a) H. Chen, I. Titushkin, M. Stroscio, M. Cho, *Biophys. J.* **2007**, *92*, 1399; b) A. Sosa-Costa, S. Isern de Val, S. Sevilla-Movilla, K. J. Borgman, C. Manzo, J. Teixido, M. F. Garcia-Parajo, *J. Biol. Chem.* **2016**, *291*, 21053.

[8] D. Valdembri, G. Serini, *Curr. Opin. Cell Biol.* **2012**, *24*, 582.

[9] a) H. Li, Z. W. Duan, P. Xie, Y. R. Liu, W. C. Wang, S. X. Dou, P. Y. Wang, *PLoS One* **2012**, *7*, e45465; b) H. Li, F. Ye, J. Y. Ren, P. Y. Wang, L. L. Du, J. L. Liu, *FASEB J.* **2018**, *32*, 5891.

[10] a) C. Jiang, B. Li, S. X. Dou, P. Y. Wang, H. Li, *Chin. Phys. Lett.* **2020**, *37*, 078701; b) B. Li, S. X. Dou, J. W. Yuan, Y. R. Liu, W. Li, F. Ye, P. Y. Wang, H. Li, *Proc. Natl. Acad. Sci. USA* **2018**, *115*, 12118.

[11] C. Cluzel, F. Saltel, J. Lussi, F. Paulhe, B. A. Imhof, B. Wehrle-Haller, *J. Cell Biol.* **2005**, *171*, 383.

[12] A. Bianchi, M. E. Gervasi, A. Bakin, *Cell Cycle* **2010**, *9*, 1647.

[13] H. Li, S. X. Dou, Y. R. Liu, W. Li, P. Xie, W. C. Wang, P. Y. Wang, *J. Am. Chem. Soc.* **2015**, *137*, 436.

[14] S. E. Leggett, A. M. Hruska, M. Guo, I. Y. Wong, *Cell Commun. Signal.* **2021**, *19*, 32.

[15] A. Kusumi, T. K. Fujiwara, R. Chadda, M. Xie, T. A. Tsunoyama, Z. Kalay, R. S. Kasai, K. G. Suzuki, *Annu. Rev. Cell Dev. Biol.* **2012**, *28*, 215.

[16] P. Moreno-Layseca, J. Icha, H. Hamidi, J. Ivaska, *Nat. Cell Biol.* **2019**, *21*, 122.

[17] J. Du, X. Chen, X. Liang, G. Zhang, J. Xu, L. He, Q. Zhan, X. Q. Feng, S. Chien, C. Yang, *Proc. Natl. Acad. Sci. USA* **2011**, *108*, 9466.

[18] E. J. Ezratty, M. A. Partridge, G. G. Gundersen, *Nat. Cell Biol.* **2005**, *7*, 581.

[19] C. M. Waterman-Storer, E. D. Salmon, *Curr. Opin. Cell Biol.* **1999**, *11*, 61.

[20] M. A. Nieto, R. Y. Huang, R. A. Jackson, J. P. Thiery, *Cell* **2016**, *166*, 21.

[21] P. Zhang, J. Meng, Y. Li, C. Yang, Y. Hou, W. Tang, K. J. McHugh, L. Jing, *Innovation* **2021**, *2*, 100174.